Realization of a causal-modeled delayed-choice experiment using single photons

Shang Yu, Yong-Nan Sun, Wei Liu, Zhao-Di Liu, Zhi-Jin Ke, Yi-Tao Wang,* Jian-Shun Tang,†
Chuan-Feng Li,‡ and Guang-Can Guo

CAS Key Laboratory of Quantum Information, University of Science and Technology of China, Hefei 230026, China and Synergetic Innovation Center of Quantum Information and Quantum Physics, University of Science and Technology of China, Hefei 230026, China

(Received 13 June 2018; revised manuscript received 24 January 2019; published 15 July 2019)

Wave-particle duality constitutes one of the most intriguing features in quantum physics. A well-known gedanken experiment that provides evidence for this is Wheeler's delayed-choice experiment based on a Mach-Zehnder interferometer [J. A. Wheeler, in *Mathematical Foundations of Quantum Theory*, edited by A. R. Marlow (Academic, New York, 1978), pp. 9–48; in *Quantum Theory and Measurement*, edited by J. A. Wheeler and W. H. Zurek (Princeton University Press, Princeton, 1984), pp. 182–213]. Many different versions of delayed-choice experiments have been conducted with both classical and quantum detecting devices. Recently, it was proposed that the delayed-choice experiment could be devised from the perspective of a device-independent prepare-and-measure scenario [R. Chaves *et al.*, Causal Modeling the Delayed-Choice Experiment, Phys. Rev. Lett. **120**, 190401 (2018)]. In our work, we experimentally realize this modified version with a deterministic single-photon source and examine the wave-particle objective in a causal-modeled scheme without the assistance of entanglement, which is achieved by violating the dimension-witness inequalities. Our experiment also provides an intriguing perspective and exhibits the benefits of studying quantum theory from the casual model point of view.

DOI: 10.1103/PhysRevA.100.012115

I. INTRODUCTION

Wave-particle duality is a central concept in quantum mechanics. Young's double-slit interference experiment [1] is a celebrated example in which the concept of duality plays an important role in the famed Bohr-Einstein debate and which prompted Bohr to formulate the complementarity principle [2]. Bohr's complementarity principle states that a single quantum object can behave as a wave or as a particle depending on the measurement apparatus. However, an alternative view of complementarity assumes that the particle somehow knows the type of detecting device and adjusts its own behavior before entering the apparatus. To examine this idea, Wheeler proposed the delayed-choice gedanken experiment where the choice of the property that will be observed is made after the photon has passed the first beam splitter of a Mach-Zehnder interferometer: "Thus one decides the photon shall have come by one route or by both routes after it has already done its travel" [3–5].

Since Wheeler's delayed-choice experiment (WDCE) was proposed, many modified versions of this experiment have been conducted [6–9]. The original version of this experiment was first realized using a fast electronic device [10,11]. Subsequently, a quantum version of the delayed-choice experiment (QDCE) was proposed by Ionicioiu and Terno [12] in a particular wave-particle objective model, where they replaced the second beam splitter in the WDCE with a quantum controlled one that could exist in a superposition of being present or absent until after the photon is detected. Ascertaining whether the beam splitter was truly in a quantum superposition state motivated an entanglement-assisted QDCE [13–15] which relied on the violation of a Bell inequality to rule out the Ionicioiu-Terno model in a device-independent (DI) manner [16,17]. Moreover, Tang *et al.* [18] observed the quantum wave-particle superposition through the interference fringes directly and proved that the quantum wave-particle superposition state was distinct from the classical mixture state because of the quantum interference between the wave and particle states.

Recently, a new proposal [19] based on the causal model demonstrated that a two-dimensional classical hidden-variable model could explain the outcomes of the WDCE and QDCE. Herein, the delayed-choice experiments could be considered from the perspective of device-independent causal models in a prepare-and-measure scenario. Furthermore, this proposal could exclude any two-dimensional nonretrocausal classical model in a device-independent manner based on the violation of the dimension-witness inequality [20,21].

In this paper we experimentally realize this causal-modeled delayed-choice experiment with a deterministic single-photon source. In order to test the wave-particle objectivity, we examine whether the hidden-variable model has the same dimension as the quantum system we test. Based on the widely used dimension-witness inequalities, we can exclude any two-dimensional nonretrocausal classical hidden-variable model in a DI manner through our experimental results and without the help of entanglement. We first test the dimension witness $|\mathrm{Det}(W_2)|$ for uncorrelated preparation-and-measurement devices where the preparation and the measurement are affected

*yitao@ustc.edu.cn
†tjs@ustc.edu.cn
‡cfli@ustc.edu.cn

 ©2019 American Physical Society

by two independent noise terms [19,20]. This method is highly robust to technical imperfections and can be used in the presence of arbitrary noise and low detection efficiency, which indicates we can test this causal-structured delayed-choice experiment in a detection loophole-free manner. Next the dimension witness I_{DW} can be obtained when the preparation and the measurement are allowed to be correlated via shared randomness. Our experimental results also show that we can violate the dimension-witness inequality in this case. Finally, we measure the retrocausality quantities at different preparation settings and show how much retrocausality would be required to reproduce the quantum experimental results. The experimental data used to violate the dimension-witness inequalities can also deduce the Hanbury Brown–Twiss [22] outcome at the same time by a different data processing method, which proves the single-photon property of our source. Our work demonstrates a WDCE in the DI prepare-and-measure scenario and shows the advantage of studying quantum theory from the causal perspective.

II. BRIEF REVIEW OF THE CAUSAL MODEL

As shown in Fig. 1(a), the causal relationships between n random variables $(X_1, \ldots, X_n)$ can be graphically described by directed acyclic graphs, where each node in the graph represents a variable and each directed edge represents a causal relation between two variables. The causal model in Fig. 1(a) implies that any observed distribution compatible with a hidden-variable (HV) causal model should be factorized as $p(d|x, y) = \sum_\lambda p(d|y, \lambda)p(\lambda|x)$. Under the assumption of nonretrocausality, the variables Y and Λ should be statistically independent. When retrocausality is allowed, there will be a causal influence between the variables Y and Λ. In Ref. [19] Chaves *et al.* proposed that the delayed-choice experiment can be regarded as a DI prepare-and-measure (PAM) scenario [Fig. 1(b)]. When pressing button X, the state preparator emits a particle in the state $\rho(x)$. Then the emitted particles are sent to the measurement device in order to perform the action of a witness. When button Y is pressed, the measurement device performs the measurements on the incoming particles and produces the outcomes. The quantum experimental results is thus described by the probability distribution $p(d|x, y)$, which can be written in the form $p(d|x, y) = \mathrm{Tr}[\rho(x)M_{d|y}]$ for the state $\rho(x)$ and measurement operator $M_{d|y}$ ($\Sigma_d M_{d|y} = \mathbb{I}$).

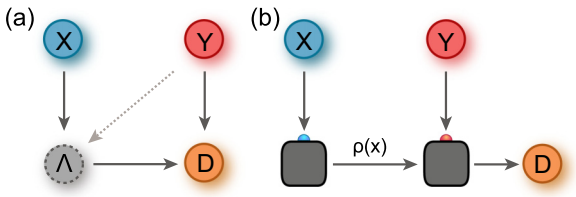

FIG. 1. Causal model and PAM scenario for the delayed-choice experiment. (a) Directed acyclic graph representation of the causal structures for the delayed-choice experiment. Under the assumption of nonretrocausality (neglecting the gray dashed line), the variables Y and Λ should be statistically independent. When the retrocausality is allowed (including the gray dashed line), there will be causal influence between the variables Y and Λ. (b) Device-independent scenario for testing the delayed-choice experiment. When button X is pressed, the state preparator emits a particle in a state $\rho(x)$ that will be sent to a measurement device. When button Y is pressed, the device performs measurement on the particle and the measurement produces outcomes D.

III. EXPERIMENTAL SETUP

The experimental setup for the causal-modeled delayed-choice experiment is illustrated in Fig. 2. Single photons generated from a hexagonal boron nitride (hBN) sample (see the Appendix for details) serve as the photon source for the experiment, which lies at the top platform in this figure. First, the photons will pass through a beam splitter (BS1), which consists of a polarizing beam splitter (PBS), a half waveplate (HWP) at 22.5°, and a beam displacer (BD), and then enter a Mach-Zehnder (MZ) interferometer. After the photons enter the interferometer, a fixed phase φ_{x_i} is immediately applied on the path a at the preparation stage, which is realized by tilting the corresponding glass plate. Then the photons are delayed by 300 ns through a 60-m-long optical fiber, which also delivers the path state $\rho(x) = |\psi(x)\rangle\langle\psi(x)|$ and $|\psi(x)\rangle = 1/\sqrt{2}(|b\rangle + e^{i\varphi_{x_i}}|a\rangle)$ to the measurement stage. It should be noted that before a photon enters the fiber, the difference of the optical length of two paths is far greater than the coherent time of the photon. Thus the fiber can be split into two isolated channels corresponding to paths a and b, according to both the coherent-time separation and polarization separation. Namely, paths a and b in the MZ interferometer are still maintained, but only propagate in the same spatial position. An attenuator in path a is used to adjust the transmittance T_a artificially. The measurement bases Y_1 and Y_2 are chosen independently by a quantum random switch (QRS), whose concrete setup is shown in the dashed line frame at the bottom of Fig. 2. The randomness of the QRS is ensured by a quantum random number generator (QRNG) [23]. The input photon in the QRS is already at the horizontal polarization for both paths since we already rotated the vertical component by a HWP at 45°. The photon then goes through a HWP at 22.5° and is focused by a convex lens pair (focal length $f = 300$ mm) into the spatial electro-optic modulator (EOM). The EOM provides a phase shift of 0 or π between the horizontal and vertical polarization according to the signal generated by the QRNG. Another HWP at 22.5° rotates the polarization again and a PBS after that can determine (according to the QRNG output) which measurement stage the photon goes to independently of the preparation. The QRS can ensure that the choice of measurement base Y does not have any causal influence from the preparation X and assists in obtaining a fast phase shift on the path degree of freedom.[1] More details about the QRS are presented in the Appendix. The phase shift σ_{y_1} or σ_{y_2} applied on path b at the measurement stage is realized by tilting the glass plate, which is similar to the preparation. The phase plates (PP) in BS2 are used to compensate for

[1]The choice of measurement stage in the QRS needs a response time around 170 ns (i.e., the phase-shift execution in the EOM is 170 ns later than the random number generated), which is shorter than the delay time after the phase is applied on path a (300 ns).

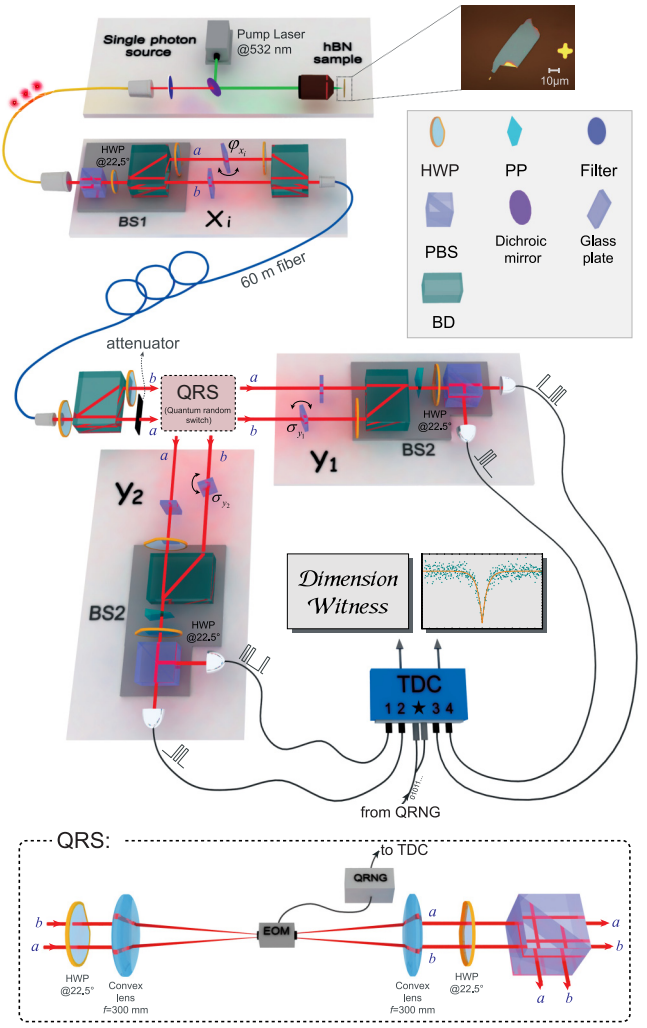

FIG. 2. Experimental setup. The single-photon source is generated from a hBN sample that is pumped by a 50-μW 532-nm laser. After the photon enters the interferometer (at BS1), a fixed phase φ_{x_i} is applied on path a by tilting the corresponding glass plate at the preparation stage. The photon is then delayed 300 ns by a 60-m-long fiber (the optical length before the fiber is unbalanced and the fiber can be split into the two isolated channels from both the polarization and coherence-time perspective). The attenuator in path a is applied to adjust the transmittance. A QRNG-based switch (QRS) inside the interferometer enables the measurement bases to be chosen independently. Two phases on the measurement stage σ_{y_1} and σ_{y_2} are realized by glass plates similar to the φ_{x_i} at the preparation stage and the photon then is detected after BS2. The HWPs are all rotated at 45° if there are no special notes. Then the dimension-witness results can be calculated from the coincidence events from ports 1, 2, and ★ for stage Y_1 or from ports 3, 4, and ★ for stage Y_2, respectively. The second-order correlation of the SPS can also be obtained by the total counts from the same data record (ports 1–4, without port ★).

undesirable phase disturbances induced by optical elements. A single-photon avalanche diode after BS2 detects the photons, which are then analyzed by a time-to-digital converter (TDC) (ID Quantique, ID800) to obtain both the dimension-witness results and the second-order time correlation of the single-photon source (SPS) simultaneously.

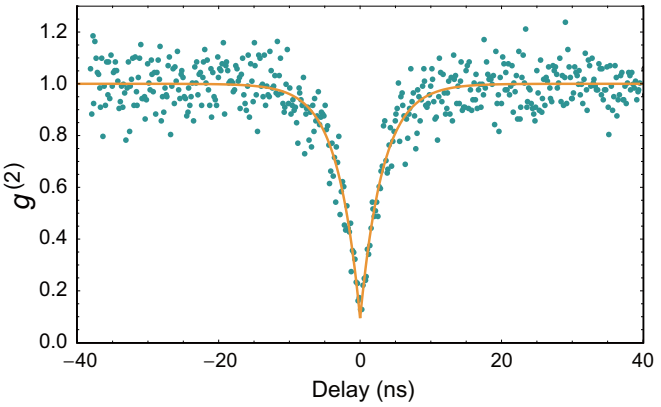

FIG. 3. Antibunching result of the SPS that is derived from the same data in experiment. The green dots are the normalized coincidence-counting results and the orange line is the theoretical fit for the data. The fitting function for the second-order time correlation is $g^{(2)}(t) = 1 - \alpha e^{-|t|/\tau}$, where t is the time delay and α and τ are the fitting parameters. The fitting results show the lifetime $\tau = 3.193 \pm 0.136$ ns.

IV. RESULTS

Figure 3 shows the antibunching result of the SPS we obtain in the experiment. Results reveal that $g^{(2)}(0) = 0.093 \pm 0.025$, and the single-photon purity then is $\sqrt{1 - g^{(2)}(0)} = 0.952$ [24], which indicates 4.8% probability of multiphoton generation in experiment. This demonstrates a remarkable quantum emission performance and the high single-photon purity at room temperature (more details can be found in the Appendix).

In order to test the wave-particle objectivity in our delayed-choice experiment, we try to rule out the two-dimensional causal-structured classical HV models, with the help of the violation of the dimension-witness inequalities. First, under the assumption that the preparation-and-measurement devices are uncorrelated, the dimension witness $|\mathrm{Det}(W_2)|$ is tested in a DI manner. Consider a scenario with $2k$ preparations and k binary measurements. We construct the $k \times k$ matrix [20]

$$\mathbf{W}_k(i, j) = p(2j, i) - p(2j + 1, i), \tag{1}$$

with $0 \leqslant i, j \leqslant k - 1$, and write $p(x, y) = p(d = 0|x, y)$ for simplicity.

Since the dimension of the HV models is 2, four preparations $\{X_i, i = 1\text{–}4\}$ and two measurements $\{Y_i, i = 1, 2\}$ are required if we try to rule out the nonretrocausal classical hidden-variable models. Thus, the matrix of interest (1) is given by

$$W_2 = \begin{pmatrix} p(0,0) - p(1,0) & p(2,0) - p(3,0) \\ p(0,1) - p(1,1) & p(2,1) - p(3,1) \end{pmatrix}. \tag{2}$$

We can find that in the two-dimensional classical hidden-variable model, the dimension witness $|\mathrm{Det}(W_2)| = 0$. In our experiment, the transmittance of path a is manipulated in the interferometer and the statistics are given by $p(x, y) = \frac{1}{4}(T_a^2 + 1) + (T_a/2)\cos(\varphi_x - \sigma_y)$. The experimental results of the dimension witness are shown in Fig. 4(a). Here four preparation bases $\varphi_{x_i} = \{0, \pi, -\pi/2, \pi/2\}$ and two measurement bases $\sigma_{y_i} = \{\pi/2, 0\}$ are chosen. Due to the nature of this

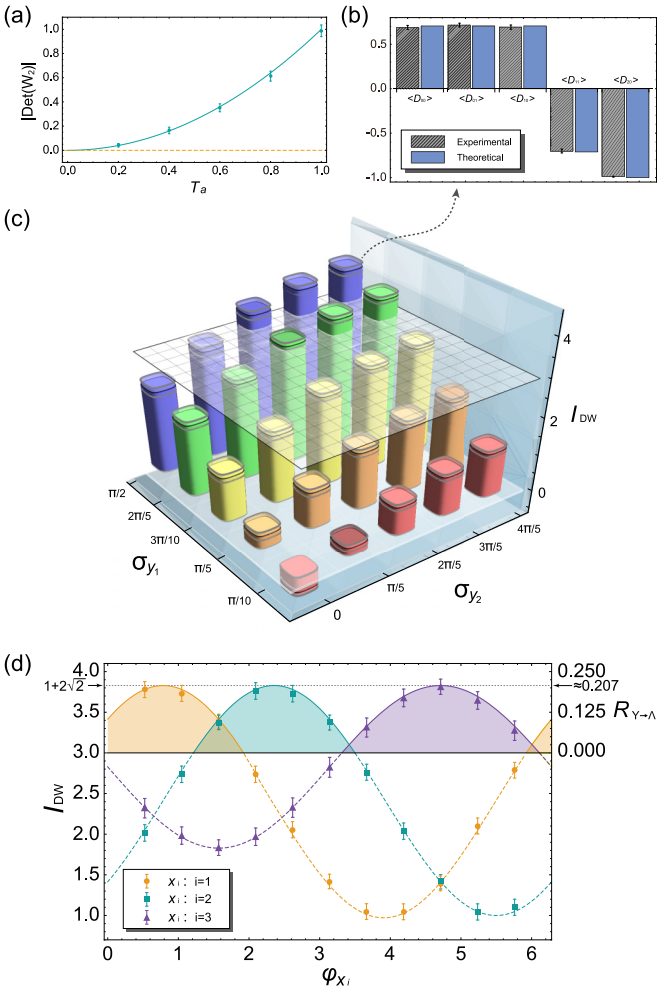

FIG. 4. Experimental results of the dimension-witness tests. (a) Experimental results of the dimension witness $|\mathrm{Det}(W_2)|$ when the real transmittance coefficients T_a of one path of the MZ interferometer is varied. (b) Results of the dimension witness I_{DW} at the maximal violation setting. Theoretical and experimental values of $\langle D_{00}\rangle$, $\langle D_{01}\rangle$, $\langle D_{10}\rangle$, $\langle D_{11}\rangle$, and $\langle D_{20}\rangle$ are illustrated, which are the terms in the dimension witness I_{DW} with maximal violation. The error bars representing one standard deviation are obtained from 30 identical experimental procedures. (c) Experimental results of the dimension witness I_{DW} with fixed phase φ_{x_i} at the preparation stage and different measurement settings. The error range of the data is represented by the two gray edges. (d) Relationship between φ_{x_i} and the retrocausality R. The lines with different colors are the theoretical values when one of the phase shifts φ_{x_i} is changed at the preparation. The orange circles, green squares, and purple triangles with error bars denote the corresponding experimental values.

dimension-witness method, we can obtain the violation under any nonzero transmittance T_a (this is equivalent to a nonideal detection efficiency situation, i.e., $\eta < 1$). By varying T_a, we find that as long as T_a is greater than zero, a dimension witness $|\mathrm{Det}(W_2)| > 0$ always exists. For the condition $T_a = 1$, the maximal violation $|\mathrm{Det}(W_2)| = 0.987 \pm 0.048$ can be obtained. These results indicate that the PAM scenario can robustly rule out the classical hidden-variable model in a DI manner and not be affected by noise and detection efficiency.

As a complement, the HV models by another dimension witness I_{DW} are also tested, for which the preparation-and-measurement devices are allowed to be correlated via shared randomness. The employed dimension-witness inequality can be written as [21]

$$I_{\mathrm{DW}} = \langle D_{00}\rangle + \langle D_{01}\rangle + \langle D_{10}\rangle - \langle D_{11}\rangle - \langle D_{20}\rangle \leqslant 3. \quad (3)$$

The experimental results of the dimension witness I_{DW} are shown in Figs. 4(b) and 4(c). In Fig. 4(c), three phase shifts $\varphi_{x_i} = \pi/4, 3\pi/4$, and $-\pi/2$ are fixed at the preparation stage and the measurement bases $Y1$ and $Y2$ are changed. From a selection of 25 examples from $\sigma_{y1} \in [0, \pi/2]$ and $\sigma_{y2} \in [0, \pi]$, only in some measurement pairs can I_{DW} be violated. The maximal violation is obtained when we set $\sigma_{y1} = \pi/2$ and $\sigma_{y2} = 0$. In this case, we obtain $I_{\mathrm{DW}} = 3.787 \pm 0.103$, which is violated by 7.6 standard deviations. The data for each value of $\langle D_{ij}\rangle$ contained in dimension witness I_{DW} are shown in Fig. 4(b). If we put aside the delayed-choice requirement, i.e., do not consider the time delay and random measurement selection, our experiment, in some aspects, is similar in structure to PAM scenarios [21] or quantum contextuality [25].

In addition, the possibility of retrocausality must be allowed if these violation results need to be simulated by a binary classical hidden-variable model. In Ref. [19] the authors proposed a retrocausality quantifier which has a direct relationship with I_{DW}. This degree of retrocausality R measurement is given by

$$\min R_{Y\to\Lambda} = \max\left[\frac{I-3}{4}, 0\right]. \quad (4)$$

Thus, according to the maximally violated I_{DW} obtained above, we can find the corresponding $R_{Y\to\Lambda} = 0.197 \pm 0.026$. The experimental results of the retrocausality $R_{Y\to\Lambda}$ under different preparations X_i are shown in Fig. 4(d). In order to determine the relationship between the preparations and the degree of retrocausality, we fix the measurement at the optimal one that is found in Fig. 4(c), i.e., $\sigma_{y_1} = 0$ and $\sigma_{y_2} = \pi/2$, and change the phase shift φ_{x_i} at the preparation stage. For example, when φ_{x_1} is changed, $\varphi_{x_{2,3}} = 3\pi/4, -\pi/2$ are kept fixed. By varying each phase shift in preparation individually, we can find, within a complete period, that the values of retrocausality $R_{Y\to\Lambda}$ are strongly influenced by preparations and always below the threshold of 0.207 within the corresponding error.

V. CONCLUSION

In this work we experimentally realized a causal-modeled delayed-choice experiment using a SPS and performed it with a MZ interferometer under a path degree of freedom. To ensure the delayed-choice requirement in the measurement stage, we built a QRS assisted by a QRNG, which can select the measurement bases independently of preparation and provides a fast phase shift at the measurement stage on the path degree of freedom. In order to test the wave-particle objectivity, in our experiment, based on the two kinds of dimension-witness inequalities $|\mathrm{Det}(W_2)|$ and I_{DW}, we examined whether the statistics property of our results is compatible with any binary classical hidden-variable model. According to our experimental results, we can exclude any two-dimensional

nonretrocausal classical models on account of the violation of the dimension-witness inequalities. In particular, results from the dimension-witness inequality $|\mathrm{Det}(W_2)|$ are highly robust to technical imperfections under any nonzero detection efficiency, which can make the test be performed in a DI manner. Meanwhile, the outcomes obtained by I_{DW} can also be applied to quantify the retrocausality, which exhibits how much information from Y to Λ (as shown in Fig. 1) that the HV model required to reproduce the quantum experimental results. In addition, results from our experiment also provide an intriguing perspective and reveal that the causal perspective can benefit studies in quantum theory.

Note added. Recently, we noticed similar works by Polino *et al.* [26] and Huang *et al.* [27], which were carried out independently.

ACKNOWLEDGMENTS

This work was supported by the National Key Research and Development Program of China (Grant No. 2017YFA0304100), the National Natural Science Foundation of China (Grants No. 11822408, No. 11674304, No. 61327901, No. 61490711, No. 11774334, No. 11774335, No. 11474267, No. 11821404, No. 11574291, and No. 91321313), the Key Research Program of Frontier Sciences of the Chinese Academy of Sciences (Grant No. QYZDY-SSW-SLH003), Anhui Initiative in Quantum Information Technologies (Grants No. AHY020100 and No. AHY060300), the Youth Innovation Promotion Association of the Chinese Academy of Sciences (Grant No. 2017492), the Foundation for Scientific Instrument and Equipment Development of the Chinese Academy of Sciences (Grant No. YJKYYQ20170032), the Fundamental Research Funds for the Central Universities (Grant No. WK2470000026), and the National Postdoctoral Program for Innovative Talents (Grant No. BX20180293).

S.Y., Y.-N.S., and W.L. contributed equally to this work.

APPENDIX

1. Details about the quantum random switch

In order to guarantee that the choice of the measurement bases has no causal influence over the preparation stage, we use a quantum random number generator to control the switch for this purpose. Before the photon enters the QRS, its polarization is rotated at the horizontal (for both paths), i.e., at state $|H\rangle$. A HWP with the optical axis at 22.5° adjusts the polarization state of the photon to $1/\sqrt{2}(|H\rangle + |V\rangle)$. A convex lens pair with a focus length of $f = 300$ mm focuses the photon in both paths into the spatial EOM. The EOM then adds a phase shift 0 or π between the horizontal and vertical polarizations, which is decided by the signal of the QRNG. The QRNG was applied in our previous work [18] and more details about how to build the QRNG can be found there. In other words, after the EOM, the polarization state of the photon at both paths will be $1/\sqrt{2}(|H\rangle + |V\rangle)$ or $1/\sqrt{2}(|H\rangle - |V\rangle)$, corresponding to the signal generated from the QRNG (0 or 1), respectively. Another HWP with the optical axis at 22.5° rotates the polarization again. If the signal generated from the QRNG is 0, and thus the polarization state of the photon is $1/\sqrt{2}(|H\rangle + |V\rangle)$, the polarization state of the photon after going through the second HWP will be $|H\rangle$ and will pass the PBS to the measurement stage $Y1$. In contrast, if the signal generated from the QRNG is 1, and thus the polarization state of photon is $1/\sqrt{2}(|H\rangle - |V\rangle)$, the polarization state of the photon after going through the second HWP will be $|V\rangle$ and it will be reflected at the PBS to the measurement stage $Y2$.

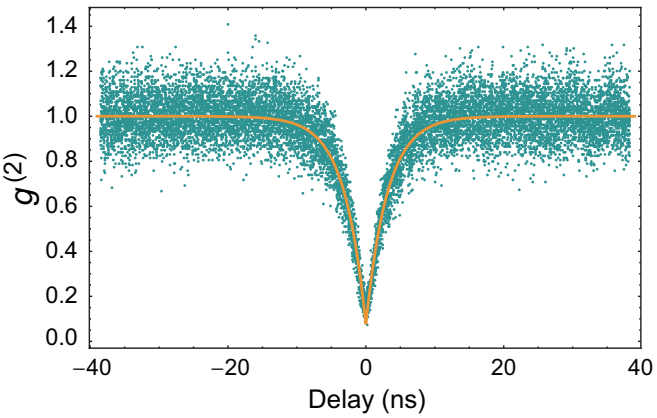

FIG. 5. Antibunching result of the SPS measured with high precision. The green dots are the normalized coincidence-counting results and the orange line is the theoretical fitting for these data. The fitting function for the second-order time correlation is $g^{(2)}(t) = 1 - \alpha e^{-|t|/\tau}$, where t is the coincidence-counting delay and α and τ are the fitting parameters.

2. Brief introduction of the hBN single-photon source

The deterministic SPS in our experiment is fabricated based on the antisite nitrogen-vacancy N_BV_N defect in hBN flakes and could maintain the stable quantum emission performance at room temperature due to the large band gap ~6 eV of hBN and the deep energy level of the N_BV_N defect [28]. To fabricate the hBN SPS, first the bulk hBN crystal (HQ Graphene) is prepared as the hBN flake by mechanical exfoliation onto the silicon wafer with the 285-nm SiO_2 layer, then the hBN sample is irradiated by the 3-keV nitrogen ion with 10^{14} ions/cm^2 to generate the N_BV_N defect, and finally the hBN sample is annealed for 30 min at 850 °C under 0.5 Torr of argon to enhance the defect stability [29]. The SPS in the hBN sample after the above processing is sought by a homemade confocal microscope, where the 532-nm continuous-wave laser is used for excitation, the objective with numerical aperture equal to 0.9 is used to focus the excitation laser and collect the sample fluorescence, and the scanning galvo system (Thorlabs, GVS012/M) is used to scan the excitation point on the hBN sample and search for the quantum emitter.

3. Fitting results with high-precision measurement

In the main text we performed the second-order photon correlation measurement with a TDC, i.e., IDQ ID800, possessing a time accuracy of 160 ps (two bins). This limited accuracy will make the dip of the coincidence counting results become vague [30]; therefore, the fitted result, i.e., $g^{(2)}(0) = 0.093 \pm 0.025$, is a little less than the minimal data value

[around at $g^{(2)}(0) = 0.12$]. Moreover, low accuracy will cause a larger step (in delay t) of the data, which may result in the minimal measured data not being exactly the zero delay (zero delay point should be the lowest data).

Here we use a high-accuracy instrument, a PicoQuanT HydraHarp 400 with a 6-ps time accuracy, to measure the antibunching results of the same hBN sample immediately after the experiment is finished. The measurement and fitting results are shown in Fig. 5.

In this situation, we find that the fitted parameters are $g^{(2)}(0) = 0.073 \pm 0.006$ and $\tau = 3.099 \pm 0.029$. Here we find that $g^{(2)}(0) = 0.073 \pm 0.006$ is not much different compared with the minimum measured value, around 0.074. This result shows that the fitted data in Fig. 3 are reasonable.

4. Details on photon generation and detection rate

In our experiment, the photon generation rate is around 100 000/s (after a 10-nm bandpass filter), the photon detection rate is around 220/s after the coincidence with the QRNG signals (this has already considered the optical path loss and coupling loss, while the random number generation rate is around 500 000/s and the coincidence window is 10 ns), and the system detection efficiency then is around 0.22%. We note that the antibunching result is obtained directly from the total data we collected at the four ports and does not coincide with the QRNG signals. It is possible to realize since we can record the data from all six ports and then calculate different quantities via different data processing methods.

[1] R. P. Feynman, R. B. Leighton, and M. L. Sands, *Lectures on Physics* (Addison-Wesley, Reading, 1965).

[2] N. Bohr, in *Quantum Theory and Measurement*, edited by J. A. Wheeler and W. H. Zurek (Princeton University Press, Princeton, 1984), pp. 9-49.

[3] J. A. Wheeler, in *Mathematical Foundations of Quantum Theory*, edited by A. R. Marlow (Academic, New York, 1978), pp. 9–48.

[4] J. A. Wheeler, in *Quantum Theory and Measurement* (Ref. [2]), pp. 182–213.

[5] A. J. Leggett, in *Compendium of Quantum Physics*, edited by D. Greenberger, K. Hentschel, and F. Weinert (Springer, Berlin, 2009), pp. 161–166.

[6] B. J. Lawson-Daku, R. Asimov, O. Gorceix, C. Miniatura, J. Robert, and J. Baudon, Phys. Rev. A **54**, 5042 (1996).

[7] Y. H. Kim, R. Yu, S. P. Kulik, Y. Shih, and M. O. Scully, Delayed "Choice" Quantum Eraser, Phys. Rev. Lett. **84**, 1 (2000).

[8] T. Hellmut, H. Walther, A. G. Zajonc, and W. Schleich, Delayed-choice experiments in quantum interference, Phys. Rev. A **35**, 2532 (1987).

[9] J. Baldzuhn, E. Mohler, and W. A. Martienssen, Wave-particle delayed-choice experiment with a single-photon state, Z. Phys. B **77**, 347 (1989).

[10] V. Jacques, E. Wu, F. Grosshans, F. Treussart, P. Grangier, A. Aspect, and J.-F. Roch, Experimental realization of Wheeler's delayed-choice gedanken experiment, Science **315**, 966 (2007).

[11] V. Jacques, E. Wu, F. Grosshans, F. Treussart, P. Grangier, A. Aspect, and J.-F. Roch, Delayed-Choice Test of Quantum Complementarity with Interfering Single Photons, Phys. Rev. Lett. **100**, 220402 (2008).

[12] R. Ionicioiu and D. R. Terno, Proposal for a Quantum Delayed-Choice Experiment, Phys. Rev. Lett. **107**, 230406 (2011).

[13] R. Ionicioiu, T. Jennewein, R. B. Mann, and D. R. Terno, Is wave-particle objectivity compatible with determinism and locality? Nat. Commun. **5**, 4997 (2014).

[14] R. Rossi, Restrictions for the causal inferences in an interferometric system, Phys. Rev. A **96**, 012106 (2017).

[15] A. S. Rab, E. Polino, Z.-X. Man, N. Ba An, Y.-J. Xia, N. Spagnolo, R. Lo Franco, and F. Sciarrino, Entanglement of photons in their dual wave-particle nature, Nat. Commun. **8**, 915 (2017).

[16] F. Kaiser, T. Coudreau, P. Milman, D. B. Ostrowsky, and S. Tanzilli, Entanglement-enabled delayed-choice experiment, Science **338**, 637 (2012).

[17] A. Peruzzo, P. Shadbolt, N. Brunner, S. Popescu, and J. L. O'Brien, A quantum delayed-choice experiment, Science **338**, 634 (2012).

[18] J.-S. Tang, Y. Li, X. Xu, G. Xiang, C. Li, and G. Guo, Realization of quantum Wheeler's delayed-choice experiment, Nat. Photon. **6**, 602 (2012).

[19] R. Chaves, G. B. Lemos, and J. Pienaar, Causal Modeling the Delayed-Choice Experiment, Phys. Rev. Lett. **120**, 190401 (2018).

[20] J. Bowles, M. T. Quintino, and N. Brunner, Certifying the Dimension of Classical and Quantum Systems in a Prepare-and-Measure Scenario with Independent Devices, Phys. Rev. Lett. **112**, 140407 (2014).

[21] R. Gallego, N. Brunner, C. Hadley, and A. Acín, Device-Independent Tests of Classical and Quantum Dimensions, Phys. Rev. Lett. **105**, 230501 (2010).

[22] R. Hanbury Brown and R. Q. Twiss, The question of correlation between photons in coherent light rays, Nature (London) **178**, 1447 (1956).

[23] J.-S. Tang *et al.*, Experimental investigation of the no-signalling principle in parity-time symmetric theory using an open quantum system, Nat. Photon. **10**, 642 (2016).

[24] R. Brouri, A. Beveratos, J.-P. Poizat, and P. Grangier, Photon antibunching in the fluorescence of individual color centers in diamond, Opt. Lett. **25**, 1294 (2000).

[25] M. D. Mazurek, M. F. Pusey, R. Kunjwal, K. J. Resch, and R. W. Spekkens, An experimental test of noncontextuality without unphysical idealizations, Nat. Commnu. **7**, 11780 (2016).

[26] E. Polino, I. Agresti, D. Poderini, G. Carvacho, G. Milani, G. B. Lemos, R. Chaves, and F. Sciarrino, Device independent certification of a quantum delayed choice experiment, arXiv:1806.00211 (2018).

[27] H.-L. Huang *et al.*, Compatibility of causal hidden-variable theories with a delayed-choice experiment, Phys. Rev. A **100**, 012114 (2019).

[28] T. T. Tran, K. Bray, M. J. Ford, M. Toth, and I. Aharonovich, Quantum emission from hexagonal boron nitride monolayers, Nat. Nanotech. **11**, 37 (2016).

[29] G. Grosso, H. Moon, B. Lienhard, S. Ali, D. K. Efetov, M. M. Furchi, P. Jarillo-Herrero, M. J. Ford, I. Aharonovich, and D. Englund, Tunable and high-purity room temperature single-photon emission from atomic defects in hexagonal boron nitride, Nat. Commun. **8**, 705 (2017).

[30] M. Reischle, G. J. Beirne, W.-M. Schulz, M. Eichfelder, R. Roßbach, M. Jetter, and P. Michler, Electrically pumped single-photon emission in the visible spectral range up to 80 K, Opt. Exp. **16**, 12771 (2008).